Marine and Petroleum Geology 98 (2018) 733–745

Contents lists available at ScienceDirect

Marine and Petroleum Geology

journal homepage: www.elsevier.com/locate/marpetgeo

Research paper

# Source to sink transport in the Oligocene Huagang Formation of the Xihu Depression, East China Sea Shelf Basin

Jingyu Zhang[a,b,c], Yongchao Lu[a,b,*], Wout Krijgsman[c], Jinshui Liu[d], Xiangquan Li[a,e], Xuebin Du[a,e], Chao Wang[f], Xiaochen Liu[g], Lin Feng[a,b], Wei Wei[a,b], Hao Lin[a,b]

[a] Key Laboratory of Tectonics and Petroleum Resources of Ministry of Education, China University of Geosciences (Wuhan), Wuhan, 430074, China
[b] Faculty of Earth Resources, China University of Geosciences (Wuhan), Wuhan, 430074, China
[c] Paleomagnetic Laboratory Fort Hoofddijk, Faculty of Geosciences, Utrecht University, Budapestlaan 17, 3584, CD, Utrecht, the Netherlands
[d] CNOOC Shanghai Branch, Shanghai, 200030, China
[e] College of Marine Science and Technology, China University of Geosciences (Wuhan), Wuhan, 430074, China
[f] Sinopec Jianghan Oilfield Branch Exploration and Development Research Institute, Wuhan, 430223, China
[g] Oil & Gas Survey, China Geological Survey, Beijing, 100083, China

ARTICLE INFO

*Keywords:*
U-Pb dating of detrital zircon
Heavy minerals
Provenance study
Sediment transport pathways
Xihu Depression
Huagang Formation

ABSTRACT

The Huagang Formation is the most important hydrocarbon reservoir in the Xihu Depression of the East China Sea Shelf Basin. Reconstructing the provenance and transport pathways of its main sand bodies is of great significance to oil and gas exploration. Previous provenance studies were mainly based on heavy mineral analyses and showed multiple source areas, but so far quantitative estimates on provenance are lacking. Detrital zircon U–Pb dating combined with heavy mineral analysis is an effective tool to quantitatively investigate sediment provenance. In this paper, we use the LA-ICP-MS method for U-Pb dating of detrital zircons of 18 samples from 13 drill cores in the Xihu Depression to determine the sediment provenance of the Oligocene Huagang sandstones. The U-Pb zircon dating results show three different age groups, in which Precambrian ages dominate (~60%), and Paleozoic and Mesozoic ages each account for ~20%. The Precambrian zircons are mainly derived from the Hupijiao uplift, which indicates a dominant and long-distance north to south transport direction. The provenance of the Paleozoic zircons is mainly from the Diaoyu Islands Folded-Uplift Belt in the east, while the Haijiao and Yushan uplifts in the west are the main source region for the Mesozoic zircons. The northern provenance transport pathway is dominated by axial channels. Incised valleys are observed in the western source and a transfer zone dominates the eastern provenance. The integration of all data results in a new schematic model of source to sink transport in the Huagang sandstones, demonstrating the complexity of multiple source rocks and sediment transport pathways in the Oligocene Xihu Depression.

## 1. Introduction

Provenance analysis is an important research component in petroleum geology. It can determine the source and character of the sediments, their transport pathways, and even the tectonic evolution of the depositional basin. The applied methods of provenance analysis, however, do not always provide solid results. It is especially difficult to quantitatively identify source areas when only based on heavy mineral and geochemical analyses (Bhatia, 1985; McLennan et al., 1993; Li et al., 2015; Pan et al., 2016; Dill and Skoda, 2017; Aubrecht et al., 2017; Licht and Hemming, 2017).

The Xihu Depression in the East China Sea Shelf Basin (ECSSB) is renowned for its rich oil and gas resources. The ECSSB is bordered by the Central Uplift Group in the west (Hupijiao, Haijiao and the Yushan uplifts), and by the Diaoyu Islands Folded-Uplift Belt in the east (Fig. 1). The Oligocene Huagang Formation (Fig. 2) is the main reservoir rock, but its provenance has been widely debated. Many provenance studies of Huagang sediments are based on heavy mineral analyses, detrital mineral composition maturity, thickness and percentage of sandstones, and seismic facies characteristics, and indicate a dominantly east-west directed transport (Xu et al., 2010; Hao et al., 2011; Gao et al., 2013). These studies conclude that the Huagang sands have mainly been derived from the Central Uplift Group and the Diaoyu Islands Folded-Uplift. Zircon U-Pb isotope dating on Huagang sediments, however,

* Corresponding author. Key Laboratory of Tectonics and Petroleum Resources of Ministry of Education, China University of Geosciences (Wuhan), Wuhan, 430074, China.
*E-mail address:* yongchaolu_2@163.com (Y. Lu).

https://doi.org/10.1016/j.marpetgeo.2018.09.014
Received 26 April 2018; Received in revised form 9 September 2018; Accepted 14 September 2018
Available online 18 September 2018
0264-8172/ 

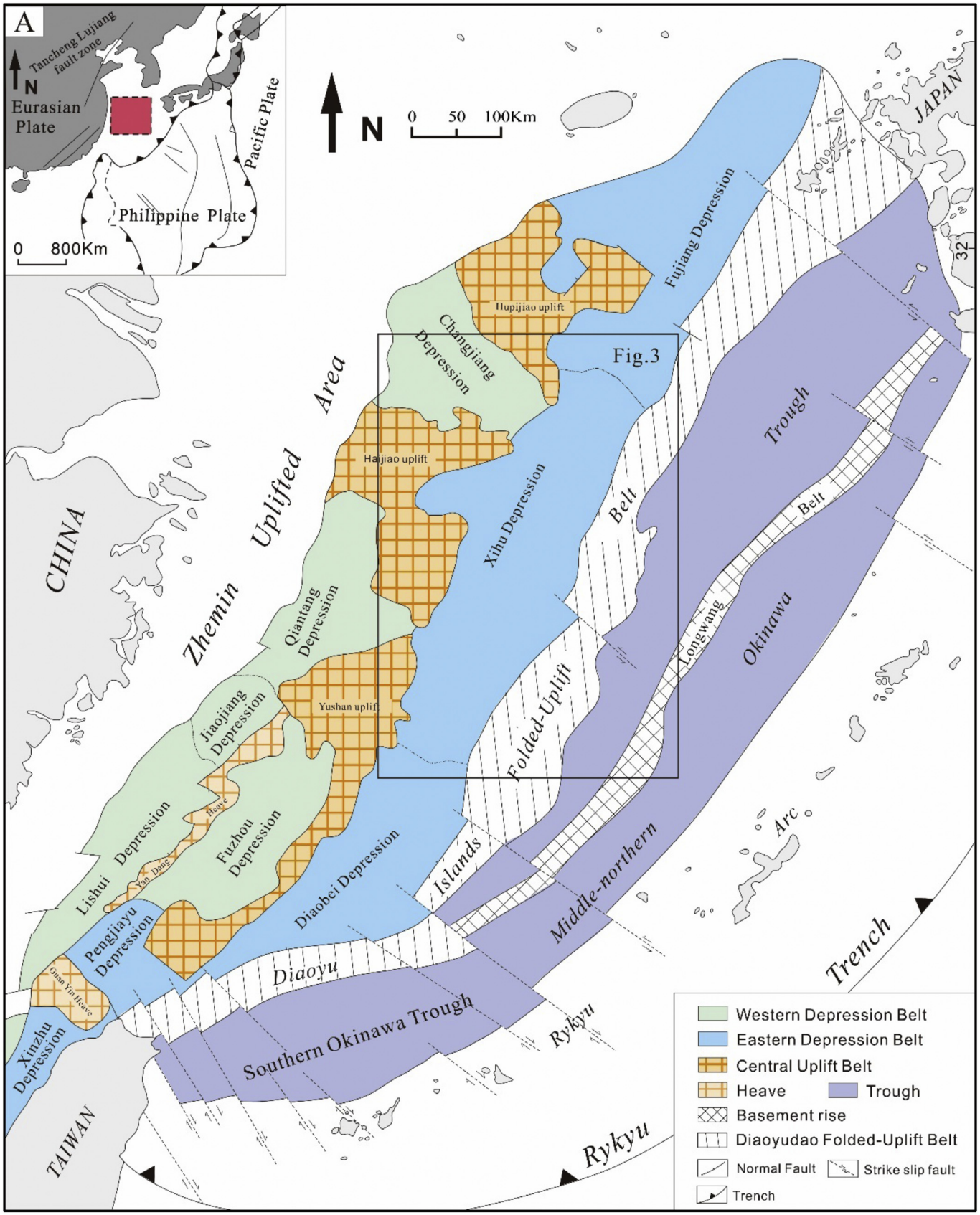


**Fig. 1.** Tectonic units of the ECSSB, modified after Zhou et al., 1989; Xu, 2012; Wang et al., 2014.

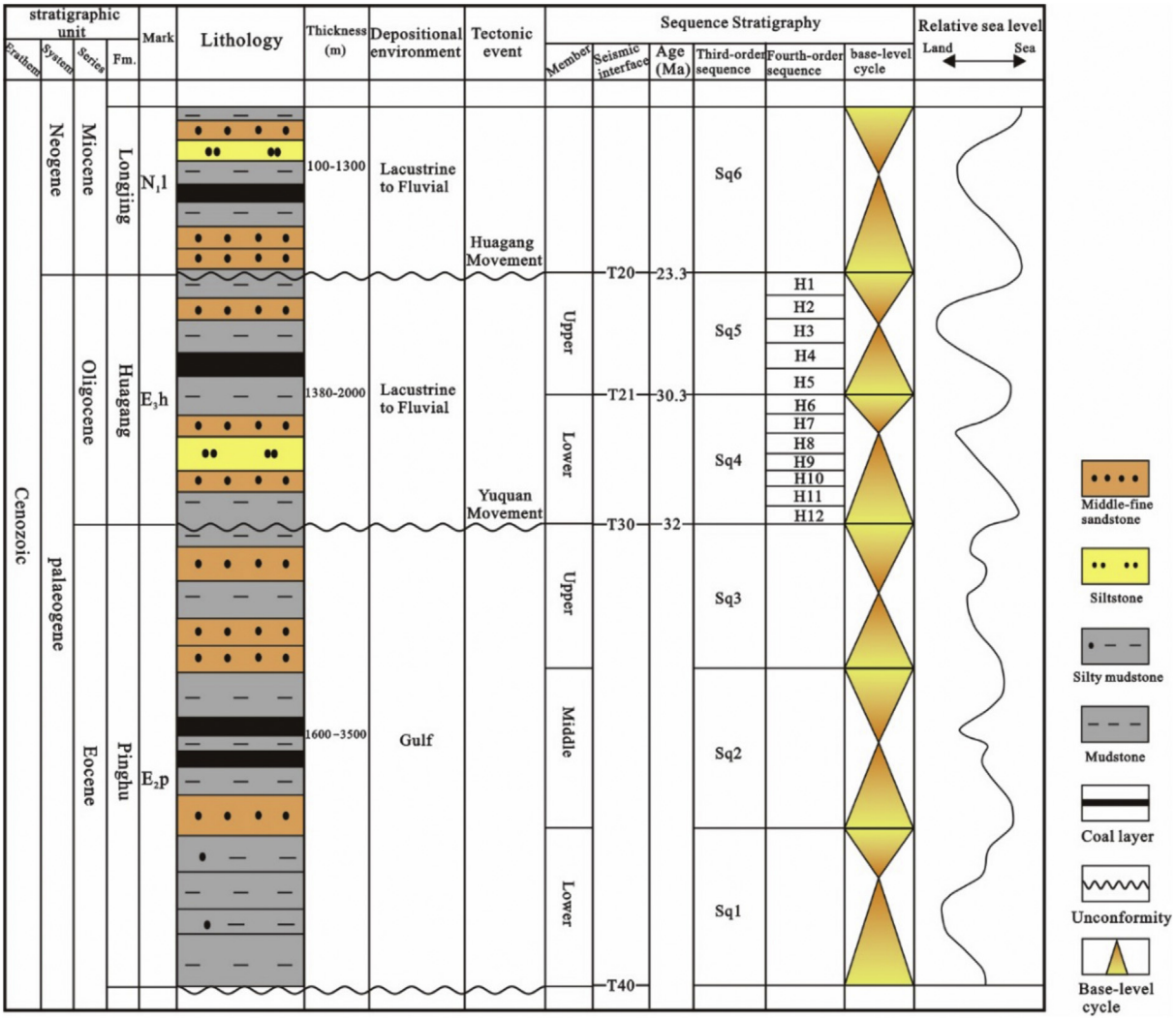


**Fig. 2.** Regional stratigraphic column and sequence stratigraphic framework of the Xihu Depression, ECSSB, modified after Zhu, 2010; Zhang et al., 2012.

revealed an additional source from the northern Hupijiao uplift (Yang et al., 2006; Qin et al., 2017). All those tools could not accurately quantify the proportion of sediment coming from the various provenance regions and consequently the exact source to sink transport in the ECSSB remains uncertain.

Here, we quantitatively determine the provenance of the Huagang sandstones and mudstones of the Xihu Depression to better understand the transport directions in the ECSSB. Our study is based on a large number of U-Pb zircon ages combined with heavy mineral analyses. We use multiple samples from several marine drill cores that are widely distributed over the basin. This allows a direct assessment in time and space of the transport pathways and sediment distribution patterns of the large sand bodies of the Huagang Formation in the Xihu Depression.

## 2. Geological background

In regional geology, the ECSSB belongs to the southeastern edge of the Eurasia plate and is located on the south China plate (including the Yangtze plate and Huaxia plate) (Fig. 1). Its formation is closely related to plate tectonic processes involving the Pacific plate, the India-Australia plate and the Philippine plate. (Zhou et al., 1989; Tao, 1994; Zhao et al., 2002; Wang, 2003; Feng et al.,.2003; Zheng et al., 2005) (Fig. 1). The closure of the Tethys Sea and the westward subduction of the Pacific Plate initiated a complex rifting phase during the late Cretaceous–Paleocene (Engebretson et al., 1985; Northrup et al., 1995; Sun et al., 2007) which progressively led to the formation of the ECSSB. The ECSSB is flanked by a series of NNE-SSW trending structural units which comprise the Zhemin uplifted area in the west and the Okinawa Trough, the Ryukyu Arc, and Ryukyu Trench in the east (Fig. 1: Yang, 1992; Yang et al., 2004).

The Xihu Depression (Fig. 1) is located in the northeastern part of the ECSSB at 124°27′–127°00′E and 27°30′–30°59′N (Liu et al., 2000; Hu et al., 2010b; Duan et al., 2017) and has a length of ~460 km, width of ~75 km–~130 km, and surface area of ~$4.6 \times 10^4$ $km^2$ (Yang et al., 2010). It forms part of a NNW-SSW trending basin system and is connected in the north to the Fujiang Depression and in the south to the Diaobei Depression (Figs. 1 and 3). The Xihu Depression is flanked by several uplifted blocks and mountain belts that form the source areas of its sedimentary basin fill. To the west of the Xihu Depression are the Haijiao and Yushan uplifts, in the north is the Hupijiao uplift and to the east stretches the Diaoyu Islands Folded-Uplift Belt. The Xihu Depression has typical characteristic of “from east to west as a belt, from south to north as a block” same as the most Mesozoic and Cenozoic fault basin in the east of China. The depression developed during three evolutionary stages: rifting-faulting (Late Cretaceous - Eocene); tectonic inversion (Oligocene - Miocene); regional subsidence (Pliocene – Quaternary) (Ye et al., 2007; Zhang et al., 2012).

The sedimentary succession of the Xihu Depression has been subdivided into numerous formations: from bottom to top these include the Baoshi, Pinghu, Huagang, Longjing, Yuquan, Liulang, Santan and

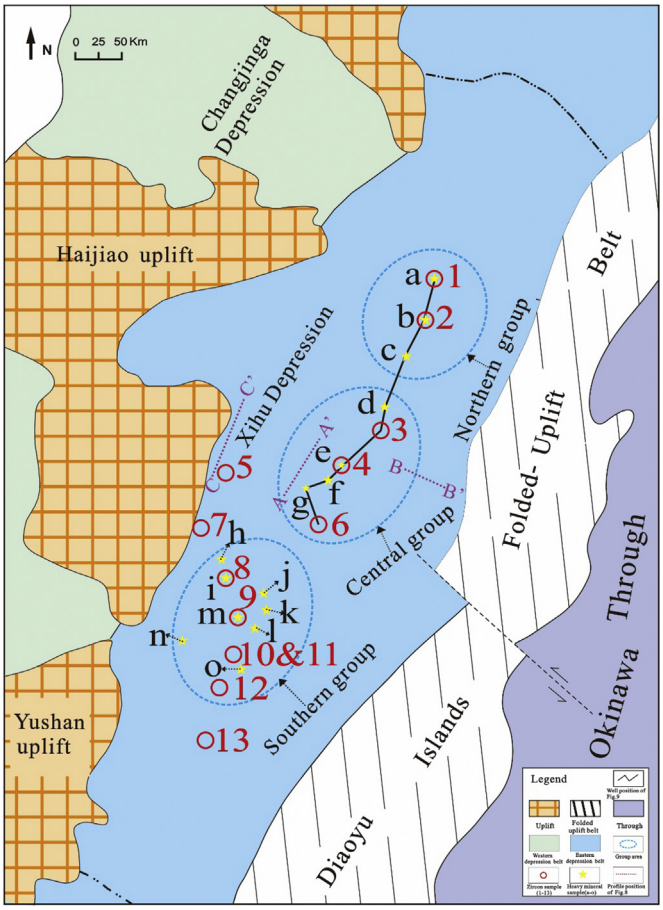


**Fig. 3.** Sample locations in the Xihu Depression, ECSSB, modified after Zhou et al., 1989; Xu, 2012; Wang et al., 2014. The red circles denote the zircon sample points (1–13). The yellow stars denote the heavy mineral sample points (a-o). (For interpretation of the references to color in this figure legend, the reader is referred to the Web version of this article.)

Donghai Formations. The total succession is approximately 10,000m thick, and is mainly composed of Paleogene and Neogene sandstones and mudstones interbedded with minor coal and limestone layers (Yang et al., 2011), Several major tectonic phases, such as the Yuquan Movement at the end of the Eocene (T30) and the Huagang Movement at the end of the Oligocene (T20), created angular unconformities in the basin (Fig. 2). The Eocene Pinghu Formation is mainly composed of siltstone, mudstone, carbonaceous mudstone and coal, indicative of tidal-flat sedimentary environments. The Oligocene Huagang Formation, the main focus of this study, was deposited between the Yuquan and Huagang Movements.

The Huagang Formation comprises an alternation of sandstones and mudstones, with some interbedded coal seams, characteristic of lacustrine, fluvial to deltaic environments (Hao et al., 2018). Recently, Zhang et al.,.2012 have recognized two 3rd order sequences within the Huagang Formation (Sq4-Sq5), which are equivalent to its lower and upper members. The lower member consists of coarse grained sediments, the upper member comprises more fine grained deposits, representing a retrogradational deposition process (Fig. 2). The Huagang Formation can furthermore be subdivided into 12 (H1-H12) forth-order sequences (Qin et al., 2017). The western margin of the basin had a relatively gentle slope and shows the development of river and delta facies deposition. The eastern margin was relatively steep and reveals mostly fan delta facies deposition (Hu et al., 2010a). A small amount of spores, pollen and charophytes have been found, suggesting that river-lake delta and shore-shallow lake deposits formed in a coastal lake or desalination bay (Wu et al., 1997).

The Miocene Longjing Formation unconformably overlies the Huagang sediments. The Longjing Formation predominantly comprises fluvial, deltaic and lacustrine sediments that were deposited during the post rift stage (Fig. 2).

## 3. Methodology

In this study, a total of 355 borehole samples of Huagang sediments, from 15 different drill core locations (a-o in Fig. 3), were collected for heavy mineral analysis. The core material was kindly provided to us by the China National Offshore Oil Corporation (CNOOC) Shanghai Branch. We calculated and summarized the average heavy mineral assemblages of all 15 locations in Table 1. Heavy mineral indices were used to analyze the heavy mineral assemblages, to study patterns of sediment transport and the influence of weathering (Morton and Hallsworth, 1994). The AB indices (ABi) were calculated using Equation (ABi = 100 x A count/(total A plus B) (Morton and Hallsworth, 1994; Guedes et al., 2011).

In addition, we selected 13 Huagang samples for zircon U-Pb geochronology analysis (Fig. 3; Table 2). We also analyzed two samples of the Eocene Pinghu and three samples of the Miocene Longjing Formations for comparison (Table 2). This resulted in a total of 1288 valid zircon ages. The color, shape and particle size of the zircon crystals were randomly selected in the sample preparation stage, to prevent potential gaps in the zircon age spectra. Data reliability was improved by increasing the number of particles of the upper and lower sample points of the target formation. The sample depth, lithology and stratigraphic horizon are shown in Table 2.

Zircon grains have been purified by hand sorting, were mounted in epoxy and polished down to approximately half sections. Cathodoluminescence (CL) image and U-Pb dating analysis were conducted by Laser Ablation Inductively Coupled Plasma Mass Spectroscopy (LA-ICP-MS) at the State Key Laboratory of Geological Processes and Mineral Resources, China University of Geosciences, Wuhan. Laser Ablation analysis was performed on a GeoLas 2005, and the ICP-MS measurements were done on an Agilent 7500a. Nitrogen was added into the carrier gas flow (Ar + He) of the Ar plasma to decrease the detection limit. Each analysis contained 20 s of gas blank followed by 50 s of data acquisition. Zircon 91,500 with an age of 1065.4 ± 0.6 Ma (Wiedenbeck et al., 1995), used as external standard for U-Pb dating, was analyzed twice every six times (Ding et al, 2017). The spot diameter was 32 μm at 1σ level of age uncertainties. We calculated U–Th–Pb isotopic ratios using the ICPMSDatacal method (Liu et al., 2008).

LA-ICP-MS analysis cannot accurately measure $^{204}Pb$ content, radioactive Pb in young zircons (< 1000 Ma) is rather weak, and the existence of common Pb will lead to great errors in test results. Therefore, data showing $^{204}Pb$ significantly higher than the background value and concordance less than 90% are eliminated from the final statistics. The $^{206}Pb/^{238}U$ age is used for young (< 1000 Ma) zircon crystals, because the amount of $^{207}Pb$ is not sufficient and may easily lead to errors. Older zircon (> 1000 Ma) crystals are expected to have relatively stable $^{207}Pb/^{206}Pb$ ratios, characteristic of synchronous changes in initial conditions and geological environment, which can be used to determine zircon formation ages (Black et al., 2003; Hu et al., 2013).

## 4. Results

### 4.1. Heavy minerals

The heavy mineral results of the 15 locations (a-o) from the Huagang Formation are given in Table 2. The heavy mineral assemblages are diverse and dominated by garnet, zircon, leucoxene, pyrite, and to a lesser extent by tourmaline, magnetite, hematite and limonite, rare mica, chlorite, epidote, titanite, rutile, barite. The samples can be

**Table 1**
Average relative percentages of heavy minerals of 15 locations (a-o) from Huagang Formation, with percentages of the ultrastable minerals (zircon, tourmaline, rutile (ZTR)). Zrn – zircon, Tur – tourmaline, Grt – garnet, Mi – mica, Chl – chlorite, Ep – epidote, Ttn – titanite, Rt – rutile, Lc – leucoxene, Mag – magnetite, Hem & Lm– hematite and limonite, Brt – barite, Py – pyrite, expressed as frequency %, GZi (garnet: zircon index), RZi (rutile: zircon index).

| Sample site | Forth-order sequence | Number | Zrn | Tur | Grt | Mi | Chl | Ep | Ttn | Rt | Lc | Mag | Hem &Lm | Brt | Py | other | ZTR | GZi | RZi |
|---|---|---|---|---|---|---|---|---|---|---|---|---|---|---|---|---|---|---|---|
| a | H1 | 4 | 4.6 | 1 | 30.5 | 1.9 | 1.3 | 2.9 | 0.4 | 0.2 | 8.1 | 22 | 22.1 | 0.1 | 4.9 | 0 | 5.8 | 86.9 | 4.2 |
| | H2 | 7 | | | | | | | | | | | | | | | | | |
| | H3 | 12 | | | | | | | | | | | | | | | | | |
| | H4 | 11 | | | | | | | | | | | | | | | | | |
| b | H3 | 31 | 7.9 | 2.4 | 62.3 | 0 | 0.1 | 0.1 | 0.1 | 3.4 | 14 | 0 | 2.4 | 5.5 | 0.5 | 1.3 | 13.7 | 88.7 | 30.1 |
| c | H3 | 6 | 3.4 | 1.3 | 31.9 | 19.6 | 2.5 | 0.5 | 0 | 0.7 | 0.5 | 8.7 | 29 | 0 | 1.6 | 0.3 | 5.4 | 90.4 | 17.1 |
| d | H3 | 8 | 3.4 | 0.6 | 78.5 | 0 | 0.1 | 0.1 | 0 | 0 | 4 | 1.6 | 1 | 0 | 10.7 | 0 | 4 | 95.8 | 0 |
| e | H3 | 69 | 5.4 | 2 | 64.5 | 0 | 0.1 | 0.1 | 0 | 0.1 | 9.8 | 1.5 | 1.7 | 0.2 | 14.6 | 0 | 7.5 | 92.3 | 1.8 |
| f | H3 | 19 | 7.8 | 2.5 | 58.3 | 0.1 | 0.1 | 0.2 | 0 | 0.1 | 12.4 | 5.7 | 2 | 3.2 | 7.6 | 0 | 10.4 | 88.2 | 1.3 |
| g | H3 | 5 | 17.5 | 3.6 | 28.8 | 0.1 | 0.2 | 0.2 | 0 | 0.1 | 21.3 | 5.8 | 0.9 | 0.3 | 21.2 | 0 | 21.2 | 62.2 | 0.6 |
| | H4 | 5 | | | | | | | | | | | | | | | | | |
| | H5 | 27 | | | | | | | | | | | | | | | | | |
| h | H4 | 2 | 8.2 | 1.8 | 59.3 | 0 | 0 | 0 | 0 | 0.1 | 12.4 | 4.9 | 1.4 | 0.4 | 11.5 | 0 | 10.1 | 87.9 | 1.2 |
| | H5 | 3 | | | | | | | | | | | | | | | | | |
| | H7 | 20 | | | | | | | | | | | | | | | | | |
| | H11 | 19 | | | | | | | | | | | | | | | | | |
| i | H5 | 5 | 8.5 | 1.7 | 58.2 | 0 | 0 | 0 | 0 | 1 | 8.7 | 3.4 | 0 | 3.6 | 14.9 | 0 | 11.2 | 87.3 | 10.5 |
| j | H2 | 2 | 21.9 | 1.3 | 29 | 0 | 0 | 0 | 0 | 0.3 | 6.3 | 3 | 1.4 | 1.8 | 35 | 0 | 23.5 | 57 | 1.4 |
| | H8 | 3 | | | | | | | | | | | | | | | | | |
| k | H3 | 5 | 12.7 | 1.3 | 59 | 0 | 0 | 0 | 0 | 0 | 9.7 | 8.7 | 5.2 | 0.9 | 2.5 | 0 | 14 | 82.3 | 0 |
| | H8 | 2 | | | | | | | | | | | | | | | | | |
| | H9 | 1 | | | | | | | | | | | | | | | | | |
| l | H5 | 5 | 19.8 | 2.3 | 25.9 | 0 | 1.5 | 0 | 0 | 0.4 | 20.8 | 8.3 | 4.2 | 4.6 | 12.3 | 0 | 22.5 | 56.7 | 2 |
| | H11 | 9 | | | | | | | | | | | | | | | | | |
| m | H9 | 6 | 18.3 | 2.6 | 47 | 0 | 0.1 | 0 | 0 | 0.8 | 13.9 | 3.7 | 4.2 | 1.6 | 7.8 | 0 | 21.7 | 72 | 4.2 |
| | H11 | 6 | | | | | | | | | | | | | | | | | |
| n | H12 | 9 | 7.8 | 2.8 | 50.7 | 0 | 0 | 0 | 0 | 0 | 8.2 | 3.2 | 0.3 | 0.1 | 26.9 | 0 | 10.6 | 86.7 | 0 |
| o | H6 | 54 | 24.8 | 1.7 | 54.9 | 0.8 | 1.8 | 2.8 | 0 | 0 | 9.2 | 0.6 | 0.2 | 1.7 | 0.1 | 1.4 | 26.5 | 68.9 | 0 |

**Table 2**
Location and stratigraphic information of 18 samples of locations (1–13) for U-Pb dating analyzed during this study. Mainly the samples of the Huagang Formation, a small number of other Formation samples for comparison. The sample positions are shown in Fig. 3.

| Sample | Depth(m) | Layer | Third-order | Forth-order | Lithology | Number | Concordance>90% |
|---|---|---|---|---|---|---|---|
| 1-(1) | 1229.1 | N1l | Sq6 | none | Silty mudstone | 20 | 18 |
| 1-(2) | 2600.98 | N1l | Sq6 | none | Mudstone | 85 | 81 |
| 2 | 3411.47 | E3h | Sq5 | H4 | Fine-sandstone | 90 | 71 |
| 3-(1) | 2622.79 | N1l | Sq6 | none | Fine-sandstone | 85 | 72 |
| 3-(2) | 3418.23 | E3h | Sq5 | H3 | Fine-sandstone | 85 | 67 |
| 4 | 3763 | E3h | Sq5 | H3 | Fine-sandstone | 85 | 80 |
| 5 | 4209.52 | E2p | Sq2 | none | Fine-sandstone | 93 | 81 |
| 6-(1) | 2346.18 | E3h | Sq5 | H1 | Mid-sandstone | 83 | 72 |
| 6-(2) | 2826.24 | E3h | Sq5 | H3 | Mid-sandstone | 88 | 83 |
| 7 | 3446.57 | E2p | Sq3 | none | Fine-sandstone | 93 | 90 |
| 8 | 3540.62 | E3h | Sq5 | H5 | Fine-sandstone | 86 | 69 |
| 9 | 3719.02 | E3h | Sq4 | H10 | Fine-sandstone | 83 | 67 |
| 10 | 2715.16 | E3h | Sq5 | H3 | Mudstone | 91 | 76 |
| 11 | 3607.78 | E3h | Sq4 | H10 | Fine-sandstone | 91 | 77 |
| 12-(1) | 2205.2 | E3h | Sq5 | H1 | Mudstone | 83 | 69 |
| 12-(2) | 3113.5 | E3h | Sq4 | H9 | Mudstone | 84 | 71 |
| 13-(1) | 2677.14 | E3h | Sq5 | H5 | Fine-sandstone | 85 | 75 |
| 13-(2) | 3227.27 | E3h | Sq4 | H12 | Fine-sandstone | 85 | 69 |

grouped based on the heavy mineral assemblages and location of the samples (Figs. 3 and 4). The samples (a, c) from the northern part of the depression show high percentages of garnet, zircon, magnetite, hematite and limonite, while the percentage of pyrite is relatively low. The samples (d, e, f, g) from the middle part show a decreasing trend in garnet percentage and an increasing trend in leucosphenite and zircon from north to south. The samples from the southern part are dominated by pyrite, zircon, leucosphenite and have the highest content of zircon (Fig. 4). They show only minor amounts of mica, chlorite, epidote and titanite.

The ZTR (zircon-tourmaline-rutile) index varies from 4% to 26.5% over the Xihu Depression. The northern group samples show the lowest ZTR values ranging between 4% and 13.7%. The westernmost samples (h, i, n) show remarkably similar values of ~11%. The samples (d, e, f, g) from the middle part of depression show again a N-S trend, with increasing ZTR index (from 4% to 21.2%). The samples in the southern part show the highest ZTR values, generally well above 20% (Table 2). All samples display relatively high GZi (garnet: zircon index) values varying from 56.7 to 95.8. The samples from the northern and central part show the highest GZi values (62.2–95.8). The westernmost samples (h, i, n) show remarkably similar values of 87. The samples in the southern part (g, j, l, m, o) show the lowest GZi values (56.7–72). The RZi (rutile: zircon index) shows relatively low values varying from 0 to 30.1. The northern samples show the highest RZi values (4.2–30.1), the central samples the lowest (0–1.8). The samples in the southern part show intermediate values (0–10.5; Table 1).

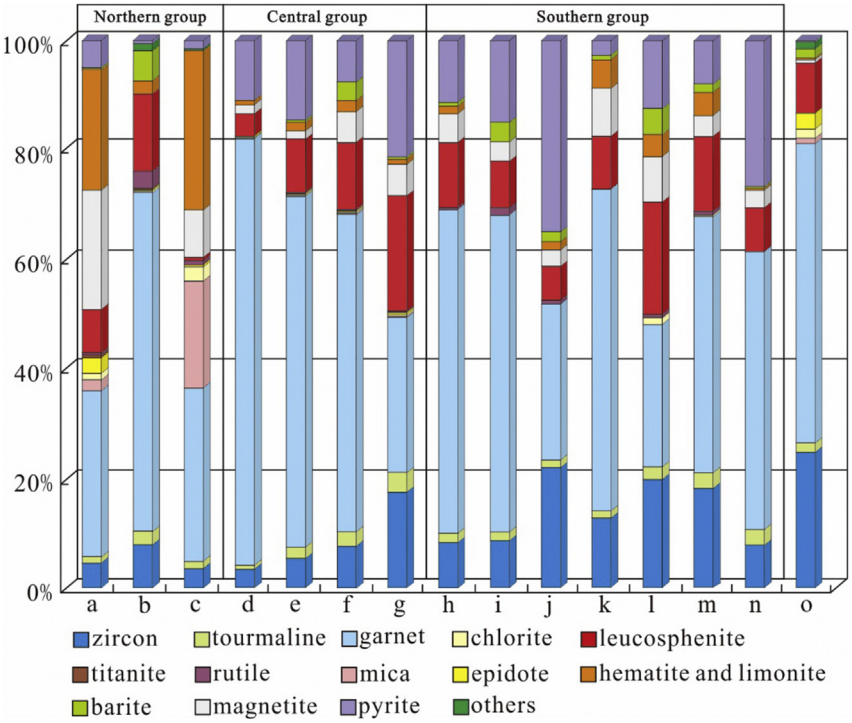


**Fig. 4.** Heavy mineral abundances of the Oligocene Huagang Formation sediments from the Xihu Depression.

### 4.2. Cathodoluminescence (CL) images of detrital zircon

Cathodoluminescence images of detrital zircons (Fig. 5) can reveal information about the inner ring and metamorphic hyperplasia, which is beneficial to the genetic analysis of the mother rock. At the same time, the U-Pb age of the zircon can be derived, which indicates the geological age of the source rock formation. Most (> 95.85%) Th/U values range 0.10–4.39, expressing a magmatic origin (Belousova et al., 2002; Lopez-Sanchez et al., 2016), the age represents the formation time. The CL images of the Precambrian zircons are relatively fuzzy and their appearance is complex. The ring belt is not always obvious and some shapes show short columns, other grains have been transported and are well-rounded (Fig. 5a). The CL images of Paleozoic zircons are mostly bright dark and show development of growth zoning and metamorphic hyperplasia. Some grain boundaries are straight and euhedral, indicating short transport distances (Fig. 5b). The CL images of Mesozoic zircons are relatively flat, and the dominant shape is cylindrical. Most of the Mesozoic zircons reveal oscillatory zoning of magmatic origin. Some particles are clearly damaged and their roundness degree varies significantly, indicating different transport distances (Fig. 5c) (Wang et al., 2016).

The grain size of the zircons of the Huagang Formation is generally in the range 50–120 μm, a few are larger than 150 μm, and the aspect ratio is 1:1-2:1. The shape of the zircons is usually subround to subangular, showing various euhedral shapes, and the degree of damage varies significantly. This indicates a mixture of short and long distance transport from multiple provenance areas (Fig. 5).

### 4.3. Detrital zircon ages

These samples are predominantly taken from the Oligocene Huagang Formation (13 samples), while 2 samples (5 and 6-2) are from the Eocene Pinghu Formation and 3 samples (1-1, 1–2 and 3-1) come from the Neogene Longjing Formation. The results are shown in U-Pb Concordia diagrams and in age distribution histograms (Fig. 6; Fig. 7). Four Huagang samples (3, 6, 10, 13), roughly located on a north to south transect, were selected to further analyze the zircon age distribution characteristics (Fig. 6). One sample of the Longjing (3-1) and one of the Pinghu (5) Formation were selected to compare with the Huagang results.

The zircon data of all 18 Xihu samples (1–13) have a wide age spectrum (Figs. 6 and 7) and show that they were derived from Precambrian to Cenozoic rocks. This implies that the source rocks also must have wide age ranges (Choi et al., 2013). The Precambrian zircon

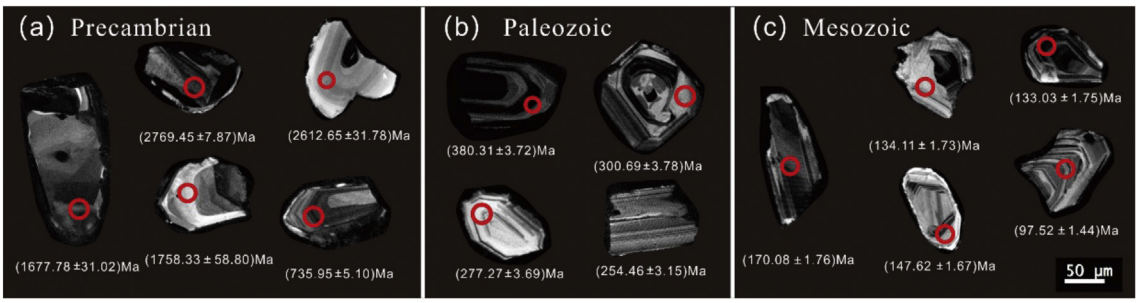


**Fig. 5.** Representative cathodoluminescence (CL) images of detrital zircons. The red circles denote the LA-ICP-MS analytical spots for U-Pb ages. Numbers near the circles are the U-Pb ages. (a)–(c) Representative CL images of detrital zircons of Precambrian to Mesozoic age. (For interpretation of the references to color in this figure legend, the reader is referred to the Web version of this article.)

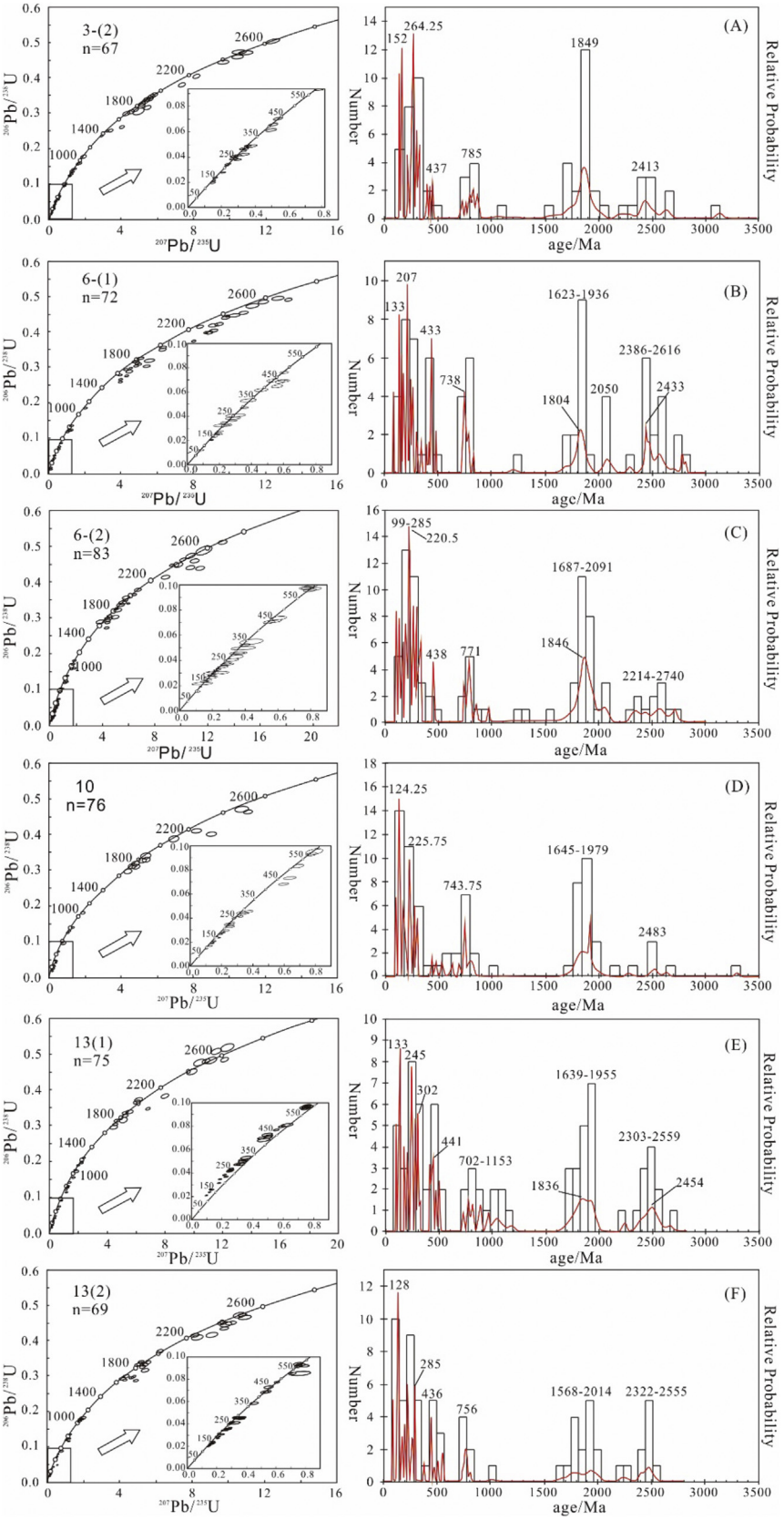


**Fig. 6.** U-Pb Concordia and histogram diagram of detrital zircons for the Huagang Formation in the ECSSB. Data-point error ellipses are 1 sigma. The numbers above the relative probability curve are the peaks of zircon U-Pb ages.

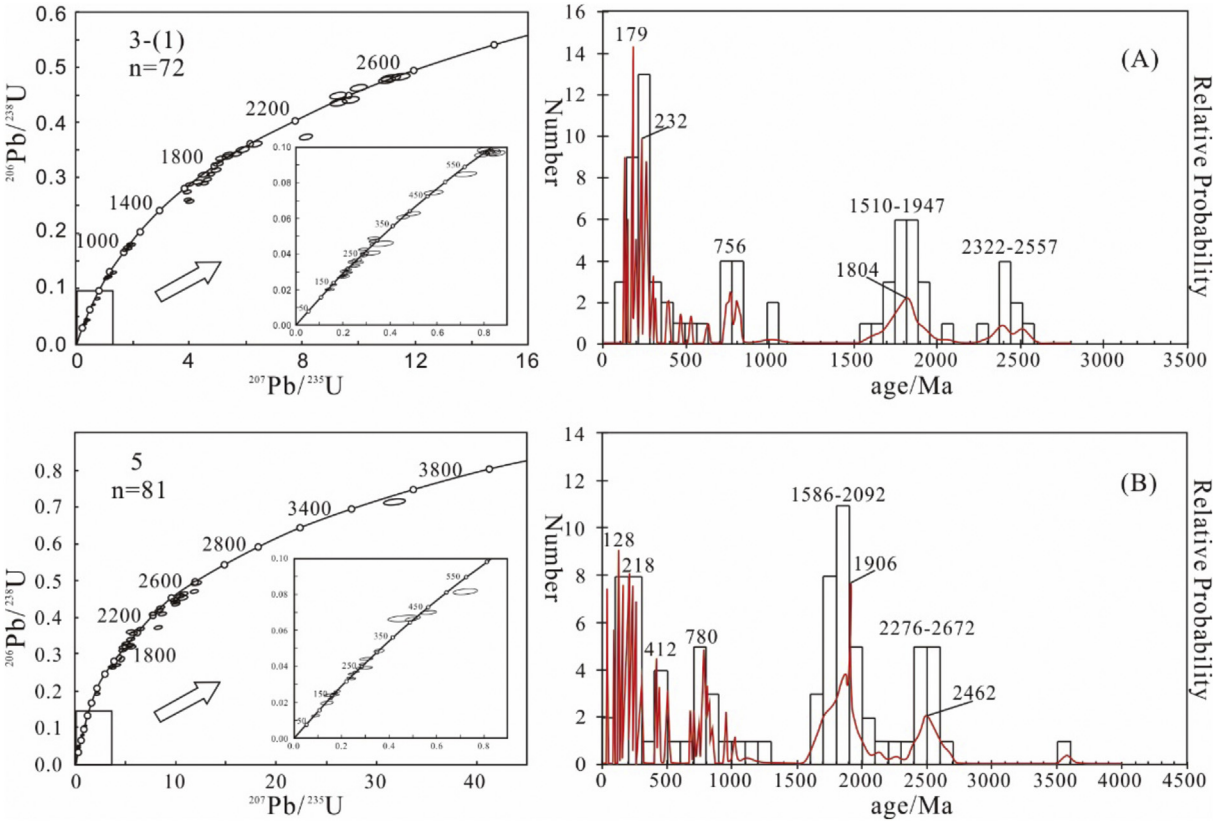


**Fig. 7.** U-Pb Concordia and histogram diagram of detrital zircons for the Longjing and Pinghu Formations in the ECSSB. Data-point error ellipses are 1 sigma. The numbers above the relative probability curve are the peaks of zircon U-Pb ages.

age dominates over 61.96% on average. The Paleozoic zircon age accounts for 17.39%, the Mesozoic age for 20.65%. There is only one Cenozoic age of 34.91 ± 0.59 Ma. The 1288 analysis points were distributed from 34.91 ± 0.59 Ma to 3577.47 ± 35.26 Ma, with four main age peaks of 130.5 Ma, 261Ma, 434Ma and 774Ma, and two main age groups of 2100-1550 Ma (main peak) and 2650-2200 Ma (subpeak). Furthermore, the results from the Pinghu, Huagang and Longjing Formations are all rather similar.

Sample 3 is located in a braided river channel area, and its grain size is 50–120 μm. The age spectrum of sample 3-(1) from the Longjing Formation shows a peak at 1804 Ma (proportion of 55.56%), a peak of 382.2 Ma (16.67%) and a peak of 232 Ma (27.77%) (Fig. 7A). The age spectrum of sample 3-(2) shows a peak at 1849 Ma (61.19%), a peak of 437 Ma (22.39%) and a peak of 264.25 Ma (16.42%) (Fig. 6A). This implies that the source rock ages were mainly Precambrian, Paleozoic and Mesozoic. Sample 5 from the Pinghu Formation reveals a peak age of 1906 Ma (70.37%), a peak of 412 Ma (9.87%), a peak of 128 Ma (18.53%) and only one Cenozoic age (1.23%) (Fig. 7B). The age spectra of the Longjing and Pinghu samples have similar distributions as the Huagang samples.

Sample 6 is located in an anastomosing river plain area, and zircon particles of sample 6-(1) are generally smaller than at 6-(2). The samples 6-(1) and 6-(2) both reveal a prominent Precambrian peak age of 1804 Ma (62.50%) and 1846 Ma (59.04%), respectively. The Paleozoic zircons reveal ages of 433 (16.67%) Ma and 438 Ma (18.07%) and the Mesozoic zircons have peaks at 207 Ma (20.83%) and 220.5 Ma (22.89%), respectively (Fig. 6B.C). This demonstrates that there is an increase of Mesozoic provenance in this area, with respect to sample 3.

The zircon particle size of sample 10 is 50–120 μm, the Precambrian peak age arrives at 1904 Ma (55.26%), the Mesozoic age at 225.75 Ma (31.58%) and the Paleozoic zircons were the least prominent, their peak age was 432.25 Ma (13.16%; Fig. 6D).

Sample 13 is located in a lacustrine delta area, sample 13-(1) zircon particles are similar in shape to sample 13-(2), and both have grain sizes of 50–130 μm. The prominent Precambrian peak ages are 1836 Ma (57.33%) and 1897 Ma (47.83%), the Paleozoic peak ages are 302 Ma (25.34%) and 285 Ma (21.74%), the Mesozoic peak ages are 133 Ma (17.33%) and 128 Ma (30.43%), respectively. It shows that the proportion (47.83%) of Precambrian zircons at sample point 13-(2) is the least of all samples in the Xihu Depression, and the proportion (30.43%) of Mesozoic zircons the highest, illustrating the influence of Precambrian provenance decreased in this southernmost area (Fig. 6E.F).

## 5. Discussion

### 5.1. Detrital zircon provenance

The U-Pb dating results show that the main source rock of the Huagang sandstones is of Precambrian age. Precambrian strata in the bedrock units surrounding the Xihu Depression are only known from the Hupijiao uplift (Proterozoic metamorphic rocks superimposed on Yanshanian igneous rocks) (Liang et al., 2006; Yang et al., 2010). There is no other uplift area with Precambrian strata. Hence, the Precambrian zircons must have been derived from this northern source region and can be named Hupijiao provenance (Qin et al., 2017). The two main other age groups in U-Pb zircon dating are Paleozoic and Mesozoic. Paleozoic metamorphic strata form the key bedrock units of the Diaoyu Islands Folded-Uplift Belt (Yang et al., 2010). The Paleozoic zircons thus indicate a source region east of the Xihu Depression, named Diaoyu provenance. Provenance of Mesozoic zircons mainly comes from a western source region, named Haijiao provenance. The exposed bedrock of Haijiao (and Yushan) uplifts are mainly composed of upper Jurassic-middle Cretaceous (Yang et al., 2010). Both the eastern and

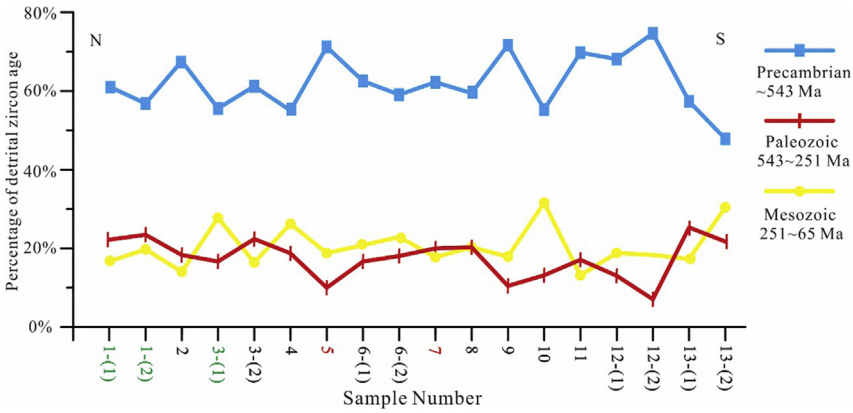


**Fig. 8.** Age proportion of all samples (1–13). The black sample numbers denote the samples from the Oligocene Huagang Formation, the red numbers denote samples from the Eocene Pinghu Formation, the green numbers indicate samples from the Neogene Longjing Formation. (For interpretation of the references to color in this figure legend, the reader is referred to the Web version of this article.)

western provenance is marked by relatively short transport distances, especially when compared to the northern provenance.

Plotting the percentages of detrital zircon age against sample location on a north to south transect shows that the percentage of Precambrian zircon ages varies around ~60% in all Xihu samples, while the Paleozoic and Mesozoic ages both have an average percentage of ~20% (Fig. 8). The detrital zircon ages of the Longjing and Pinghu samples both reveal a major Precambrian contribution and a small Paleozoic-Mesozoic contribution, similar to the Huagang samples (Figs. 7 and 8). This confirms the reliability of the Huagang data and the stability of the source supply in the Xihu Depression.

The Precambrian zircon percentage, indicating a northern Hupijiao provenance, is remarkably stable over the main part of the Huagang Formation in the entire Xihu Depression. Only the southernmost locality (13-(1) and 13-(2)) show lower values, this sample is also furthest away from the Hupijiao provenance (Fig. 8). The Paleozoic-Mesozoic percentages show small differences over the N-S transect. Samples from the northern group (1, 2; Fig. 3) show the lowest values of Mesozoic zircons, while the samples from the middle group (3–6; Fig. 3) show higher Mesozoic values than Paleozoic values. This implies that the eastern Diaoyu provenance is more important in the northern region, while the contribution of the western Haijiao provenance slightly increases in the central part of the Xihu basin. The influence of Mesozoic parent rock in the Huagang Formation increased near the Haijiao uplift. The percentage of Mesozoic zircons is the highest in sample 10, which may be related to co-influence of Haijiao uplift and Yushan uplift.

### 5.2. The response characteristics of the heavy mineral assemblages to the provenance

Heavy mineral assemblages of clastic rocks are also influenced by the transport distance of detritus from the provenance source. They can be sub-divided into ultrastable heavy minerals (zircon, tourmaline, rutile), stable minerals, and unstable heavy minerals according to their resistance against weathering effects (Hubert, 1962). The zircon-tourmaline-rutile (ZTR) index, the percentage of combined zircon, tourmaline, and rutile grains to total heavy minerals, is considered a useful stability proxy that can be used as indicator for transport distance and direction (Hubert, 1962). GZi and RZi are provenance-sensitive heavy mineral ratios that can be applied in sandstone provenance analysis (e.g., Morton et al., 2004, 2005; Hallsworth and Chisholm, 2008; Guedes et al., 2011; Jian et al., 2013), because rutile and zircon (RZi) have similar physical and chemical properties. Garnet and zircon (GZi) reflect the stability of garnet and the variation of parent rock composition in the source area (Morton and Hallsworth, 1994, 1999).

Generally, the sediments from the same denudation area often have similar heavy mineral assemblages and percentages. The unstable mineral content in the sediments, however, gradually decreases with increased transport distance (Morton and Hallsworth, 1994; Zhu et al., 2017). On the other hand, ultrastable heavy mineral content generally increases with distance from the source (Morton et al., 1999; Zhu et al., 2017).

Our heavy mineral data show that garnet, leucosphenite, pyrite, zircon are the main components in the Huagang Formation (Table 2; Fig. 4). The samples from the northern group (a-c; Fig. 3) show different patterns, as the heavy mineral assemblage of sample (a) shows remarkably high values of magnetite, hematite and limonite, and sample (c) shows anomalously high values of mica, hematite and limonite. The percentages and assemblages of heavy mineral varies in each sample, indicating that the northern region of the Xihu Depression was a multiple provenance mixing zone (Tang et al., 2017). The RZi index shows varying values in the northern group (4.2–30.1), central group (0–1.8) and southern group samples (0–10.5), confirming the hypothesis of multiple source areas in the Xihu Depression.

The samples from the central group (d-g; Fig. 3) all have similar heavy mineral assemblages (mainly garnet, zircon, leucosphenite, pyrite, magnetite), but there are marked changes in relative percentage. The percentage of garnet clearly decreased from north to south, while the percentages of pyrite, leucosphenite, zircon generally increased (Fig. 4). This can be explained by the influence of northern provenance generally decreasing as the transport distance increased. A similar trend is observed in samples h, i, j, of the southern group that are roughly located on a west to east transect. The percentage of garnet and leucospenite decreases from west to east, while the percentage of zircon increases, in agreement with the increased distance from a western provenance source.

The GZi index displays relatively high values (56.7–95.8) over the Xihu Depression, indicating a stable supply of Metamorphic rocks. The relatively low GZi (56.7–72) of the southern samples (g, j, l, m, o) show a decrease of impact of Metamorphic rock provenance in this area. The samples that are closer to the Hupijiao uplift or near to the Haijiao uplift show relatively high values (> 82) (Table 2).

The ZTR index is lowest in the northern (a-f) and westernmost (h,i,n) samples of the Xihu Depression (Table 2). The samples of the northern depression are closest to the Hupijiao uplift and are near the Diaoyu Islands. The low ZTR index (~10%) of the westernmost samples (h, i, n,) are in agreement with a nearby source and supply of western Haijiao provenance. The samples (d-g) in the middle part of the Xihu Depression show a north to south increase in the ZTR index, confirming a gradual increase in transport distance from a northern provenance. The ZTR index of the samples (j-o) located in the central part of the southern depression are the highest (> 20%), indicating this area is located furthest from the provenance source (Table 2).

### 5.3. Multiple transport pathways from source to sink

The sediment transport pathway from source to sink plays a very important role in provenance studies. We have shown that there existed

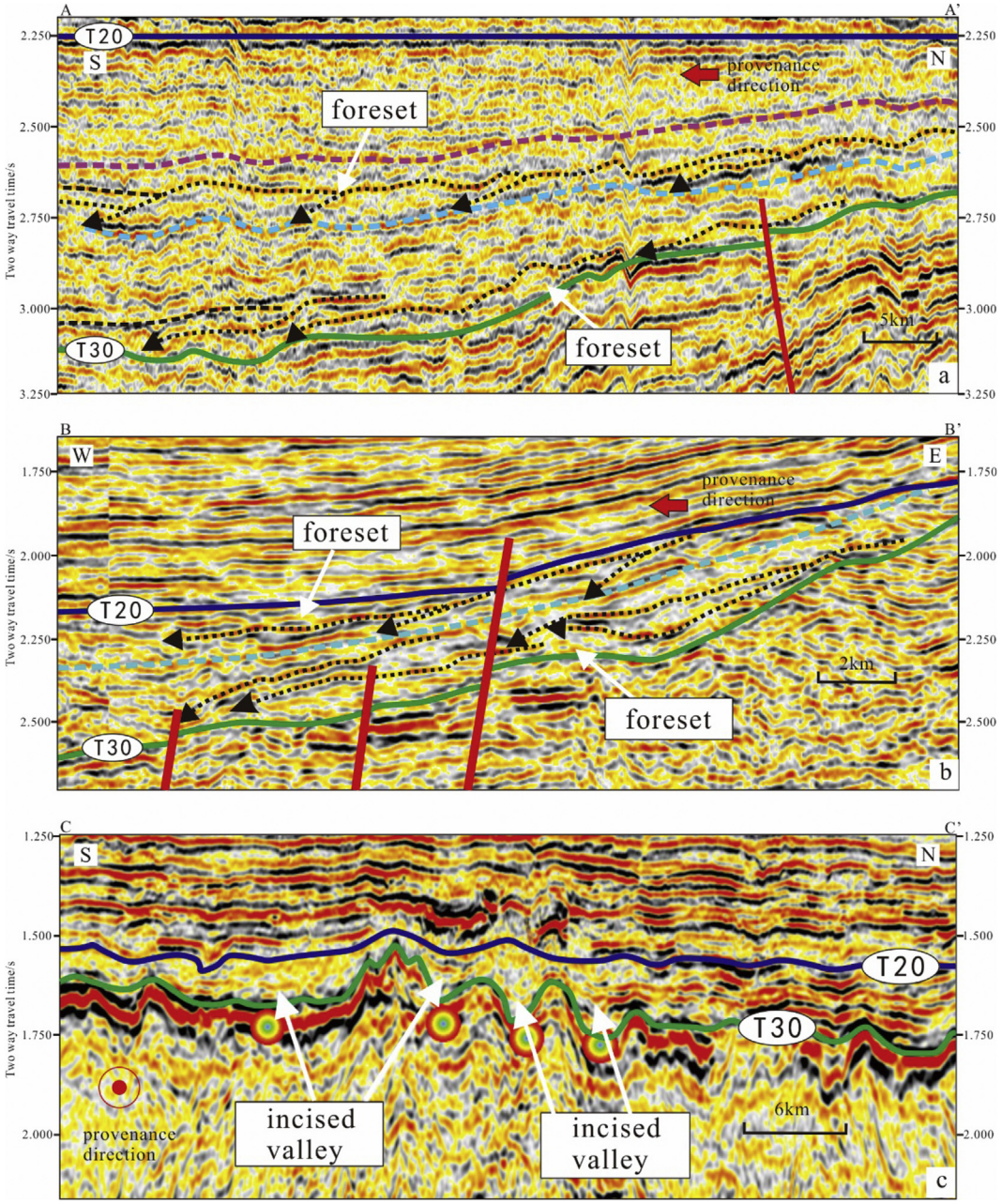


**Fig. 9.** Corresponding interpretation of the seismic profiles. (a) The axial channel is shown as progradational reflection configuration from north to south; (b) The progradational reflection configuration is also identified under the control of the transfer zone from east to west; (c) The incised valleys are identified from north to south. The approximate locations of seismic profile are shown in Fig. 3.

at least three provenance directions in the Xihu Depression, a northern, western and eastern source. There are furthermore multiple types of transport pathways, like axial channels, incised valleys and transfer zones, which all have their own characteristics.

Many researchers have previously studied sediment transport progress in axial channels, showing this can be an efficient transport pathway (e.g. Paull et al., 2002; De Stigter et al., 2007). Seismic profiles in the Xihu Depression show the axial channel is an important pathway that controls the input of the northern Hupijiao provenance. The channel is probably dish-shaped, narrow at the base and wide at the top (Qin et al., 2017). The low dip and subdued topography may promote long distance sediment transport (Wu et al., 2017). The seismic profiles that are available for the region show a major sand body with obvious characteristics of a progradational reflection configuration of high amplitude and good continuous filling of the axial channel from north to south (Fig. 9a).

The well correlation section (black line in Fig. 3) was selected to show the spatial distribution patterns of the sand body and the sediment transport in a sequence stratigraphic framework. Based on the analysis of sequence stratigraphy (Zhang et al., 2012; Qin et al., 2017), lowstand systems tracts (LST) and transgressive systems tracts (TST) were recognized in Sq4 and Sq5 (Fig. 9). The distribution pattern of the main axial sand bodies is visualized by connecting the thick sand bodies in the individual wells to show the trend and direction of transport in the northern part of the Xihu Depression. The progradation and sand body migration took place from north to south. In the upstream region, the sand body is relatively thick, whereas downstream it gradually becomes branched and the bed thickness decreases (Fig. 10). This shows that transport ability along the axial channel gradually weakened with increasing distance from the source.

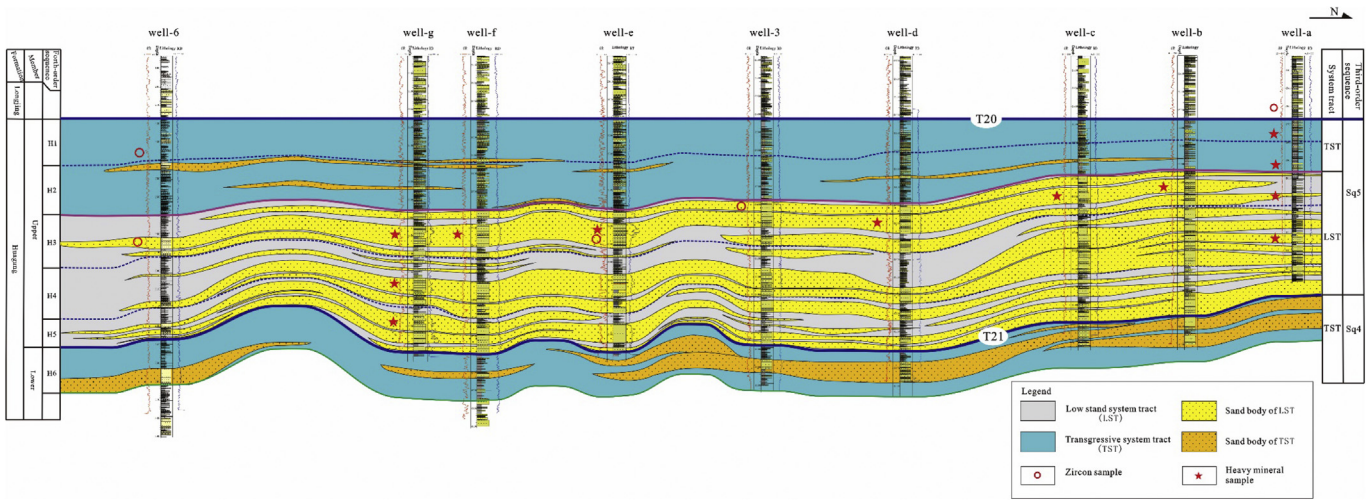


**Fig. 10.** Sequence stratigraphic correlation section from multiple wells in the Xihu Depression show the distribution characteristics of sand bodies in the Huagang Formation. The location of the wells is shown in Fig. 3. The red circles denote the zircon sample points. The red stars denote the heavy mineral sample points. (For interpretation of the references to color in this figure legend, the reader is referred to the Web version of this article.)

Transfer zones commonly develop in the background of extensional domains (Morley et al., 1990; Nelson et al., 1992). They are accommodation structures with a certain size and extension. The eastern boundary of the Xihu Depression is considered to be controlled by a segmented transform fault (Wang et al., 2011). Its control faults are steep and there are signs of strike-slip, a typical response to a transform fault. The seismic profiles of the Xihu Depression show east-west progradational phenomena exiting in many stages (Fig. 9b). This demonstrates that the eastern provenance from the Diaoyu Islands Folded-Uplift Belt transport into the Xihu Depression occurred through a transfer zone.

The analysis of seismic profiles and the reconstructed palaeogeomorphology furthermore identify many incised valleys in the western margin of the Xihu Depression, which control the input of Haijiao and Yushan provenance. The shape of these incised valleys are mainly “V” and “U” types (Chen, 2017). The sand bodies filling the incised valleys display onlap phenomena in both east and west directions (Fig. 9c). The incised valleys are commonly interpreted as elongate erosional features, with erosion and sediment transport promoted by rivers (Dalrymple et al., 1994). Incised valleys are characteristic for long distance and dendritic distribution of sediment. They usually have higher sediment discharge, which may lead to larger and thicker sand bodies. There are also some incised valleys which have characteristics of short transport distance, with a single dendritic shape parallel to the main valleys. These incised valleys are of relatively small scale, but they are large in numbers, so they may constitute a significant contribution to the provenance transport pathways.

The sink area is where the sediments finally accumulate in the depression, generally it is the deepest zone in the center of the basin. Based on this study on provenance sources, the palaeogeomorphologic reconstructions obtained from seismics, and previous research, a provenance model is proposed showing the simplified paleogeographic and source to sink patterns of the Oligocene Huagang Formation in the Xihu Depression (Fig. 11).

## 6. Conclusions

In this study, the multiple provenance characteristics of the Huagang Formation of the Xihu Depression have been clarified by combined heavy mineral assemblages and provenance analysis of detrital zircon U-Pb geochronology. The results show that:

1. The heavy mineral assemblages in the Huagang Formation are generally dominated by garnet, zircon, leucoxene and pyrite, and to a lesser extent by tourmaline, magnetite, hematite and limonite, mica, chlorite, epidote, titanite, rutile and barite. Some individual samples have different characteristics and RZi index values, indicating that the sediment input came from multiple directions and various source areas. The GZi index shows stable supply of Metamorphic rock provenance. The ZTR index shows a gradual increase from north to south and is relatively low near the western uplift area. In general, the northern provenance is dominant (~60%), and the eastern and western provenance are roughly equal (both ~20%).
2. U-Pb dating of detrital zircons from the Oligocene Huagang Formation indicates Precambrian ages dominate (> 61.96% on average), Mesozoic ages account for 20.65%, and Paleozoic ages for 17.39%. There are four age peaks of 130.5 Ma, 261Ma, 434Ma and 774Ma, and two age groups of 2100-1550 Ma (main peak) and 2650-2200 Ma (subpeak).
3. Combined analysis of detrital zircon U-Pb ages and heavy mineral assemblages shows that there are three different provenance directions in the Huagang Formation. The Precambrian zircons are derived from the Hupijiao uplift in the north. This Hupijiao provenance provided long-distance sediment transport from north to south. The Paleozoic zircons are mainly derived from Diaoyu Islands Folded-Uplift Belt in the east. The Mesozoic zircons are derived from the Haijiao (and Yushan) uplift, which provides short-distance sediment transport from the west.
4. The surrounding provenance is transported into the main sink areas of the Xihu Depression through multiple types of provenance transport pathways such as axial channels (northern source), incised valleys (western source) and transfer zones (eastern source).
5. The combination and integration of provenance analyses, transport pathways and seismic interpretation resulted in a schematic paleogeographic reconstruction of the source to sink distribution patterns of the Oligocene Huagang Formation in the Xihu Depression.

## Acknowledgements

We thank anonymous reviewers and journal editor Ph.D. Davide Lenaz for their specific comments and instructive suggestions. This research was funded by National Science Foundation of China (41690131), National Science and Technology Major Project of China (2016ZX05027-001 and 2017ZX05049-004). We thank CNOOC Shanghai Branch for providing valuable opportunity for sampling and

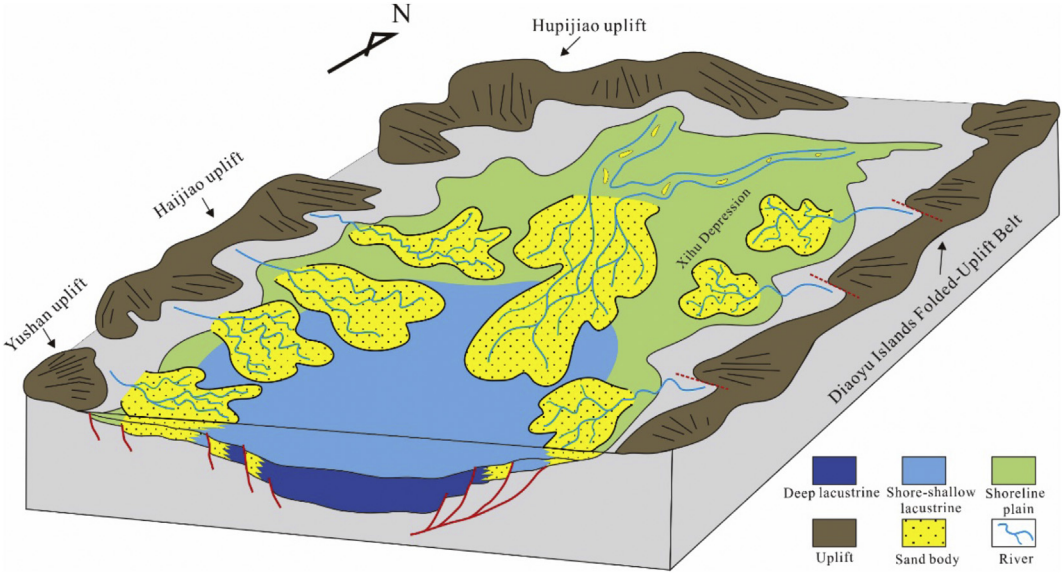


**Fig. 11.** Simplified paleogeographic scenario of the Oligocene Huagang Formation, showing the source to sink transport pathways in the Xihu Depression.

geological data.

## References


Aubrecht, R., Sýkora, M., Uher, P., Li, X.H., Yang, Y.H., Putiš, M., Plašienka, D., 2017. Provenance of the Lunz formation (Carnian) in the western Carpathians, Slovakia: heavy mineral study and in situ LA–ICP–MS U–Pb detrital zircon dating. Palaeogeogr. Palaeoclimatol. Palaeoecol. 471, 233–253.

Belousova, E., Griffin, W.L., O'Reilly, S.Y., Fisher, N.L., 2002. Igneous zircon: trace element composition as an indicator of source rock type. Contrib. Mineral. Petrol. 143 (5), 602–622.

Bhatia, M.R., 1985. Rare earth element geochemistry of Australian Paleozoic graywackes and mudrocks: provenance and tectonic control. Sediment. Geol. 45 (1–2), 97–113.

Black, L.P., Kamo, S.L., Allen, C.M., Aleinikoff, J.N., Davis, D.W., Korsch, R.J., et al., 2003. Temora 1: a new zircon standard for phanerozoic u–pb geochronology. Chem. Geol. 200 (1), 155–170.

Chen, P., 2017. Review of incised valley. Adv. Geosci. 7 (01), 67.

Choi, T., Lee, Y.I., Orihashi, Y., Yi, H.I., 2013. The provenance of the southeastern Yellow Sea sediments constrained by detrital zircon U–Pb age. Mar. Geol. 337, 182–194.

Dalrymple, R.W., Boyd, R., Zaitlin, B.A., 1994. History of Research, Types and Internal Organisation of Incised-valley Systems: Introduction to the Volume.

De Stigter, H.C., Boer, W., de Jesus Mendes, P.A., Jesus, C.C., Thomsen, L., van den Bergh, G.D., van Weering, T.C., 2007. Recent sediment transport and deposition in the Nazaré Canyon, Portuguese continental margin. Mar. Geol. 246 (2–4), 144–164.

Dill, H.G., Skoda, R., 2017. Provenance analysis of heavy minerals in beach sands (Falkland Islands/Islas Malvinas)–A view to mineral deposits and the geodynamics of the South Atlantic Ocean. J. S. Am. Earth Sci. 78, 17–37.

Ding, Ruxin, Zou, Heping, Min, Kyoungwon, Yin, Feng, Du, Xiaodong, Ma, Xuxuan, Su, Zhangxin, Shen, Wenjie, 2017. Detrital zircon U-Pb geochronology of Sinian–cambrian strata in the eastern Guangxi area, China. J. Earth Sci. 28 (2), 295–304.

Duan, M., Ye, J., Wu, J., Shan, C., Lei, C., 2017. Overpressure formation mechanism in xihu depression of the east China sea shelf basin. Earth Sci. 42 (1), 1935 (in Chinese with English Abstract).

Engebretson, D.G., Cox, A., Gordon, R.G., 1985. Relative Motions between Oceanic and Continental Plates in the Pacific Basin. Geological Society of America Special Paper 206. pp. 1–59.

Feng, X.J., Cai, D.S., Wang, C.X., Gao, L., 2003. The Meso-Cenozoic tectonic evolution in the East China Sea continental shelf basin. China Offshore Oil Gas 17 (1), 33–37 (in Chinese with English Abstract).

Gao, Y.F., Fu, H., Ge, H.B., Zhao, L.X., Xu, F.H., 2013. Provenance analysis of pinghu-Huagang Formation in xihu sag, east China sea. Sci. Technol. Eng. 22, 6549–6552.

Guedes, C.C.F., Giannini, P.C.F., Nascimento Jr., D.R., Sawakuchi, A.O., Tanaka, A.P.B., Rossi, M.G., 2011. Controls of heavy minerals and grain size in a holocene regressive barrier (ilha comprida, southeastern Brazil). J. S. Am. Earth Sci. 31 (1), 110–123.

Hallsworth, C.R., Chisholm, J.I., 2008. Provenance of late Carboniferous sandstones in the Pennine Basin (UK) from combined heavy mineral, garnet geochemistry and palaeocurrent studies. Sediment. Geol. 203, 196–212.

Hao, L.W., Liu, C., Wang, Q., Wang, H., Ma, X.F., Tang, J., Liao, P., 2011. Provenance characteristics of Huagang Formation (Paleogene) in xihu sag, east China sea. Nat. Gas Geosci. 22 (2), 315–323 (in Chinese with English abstract).

Hao, L.W., Wang, Q., Tao, H.F., Li, X.Y., Ma, D.X., Ji, H.J., 2018. Geochemistry of oligocene huagang formation clastic rocks, xihu sag, the east China sea shelf basin: provenance, source weathering, and tectonic setting. Geol. J. 53.

Hu, B., Zhai, M.G., Peng, P., Fu, L., Chunrong, D., 2013. Late paleoproterozoic to neoproterozoic geological events of the north China craton: evidences from la-icp-ms u-pb geochronology of detrital zircons from the cambrian and jurassic sedimentary rocks in western hills of beijing. Acta Petrol. Sin. 29 (7), 2508–2536.

Hu, M.Y., Ke, L., Liang, J.S., 2010a. The characteristics and pattern of sedimentary facies of huagang formation in xihu depression. J. Oil Gas Technol. 32 (5), 1–5 (in Chinese with English Abstract).

Hu, W.S., Chai, H.D., Li, R.S., Xu, F., Ge, H.P., 2010b. Application of balanced section technique to the study of positive inversion structure and hydrocarbon accumulation control in Xihu Depression of East China Sea. Special Oil Gas Reservoirs 17 (1), 15–20 (in Chinese with English Abstract).

Hubert, J.F., 1962. A zircon-tourmaline-rutile maturity index and the interdependence of the composition of heavy mineral assemblages with the gross composition and texture of sandstones. J. Sediment. Res. 32 (3).

Jian, X., Guan, P., Zhang, D.W., Zhang, W., Feng, F., Liu, R.J., et al., 2013. Provenance of tertiary sandstone in the northern qaidam basin, northeastern Tibetan plateau: integration of framework petrography, heavy mineral analysis and mineral chemistry. Sediment. Geol. 290 (1), 109–125.

Li, G., Yan, W., Zhong, L., Xia, Z., Wang, S., 2015. Provenance of heavy mineral deposits on the northwestern shelf of the South China Sea, evidence from single-mineral chemistry. Mar. Geol. 363, 112–124.

Liang, R., Zheng, Y., Wang, K., 2006. Study on magnetic anomalies in the Hupijiao reef and adjacent sea areas in the northern east China sea [J]. Adv. Mar. Sci. 24 (2), 173–180 (in Chinese with English Abstract).

Licht, K.J., Hemming, S.R., 2017. Analysis of Antarctic glacigenic sediment provenance through geochemical and petrologic applications. Quat. Sci. Rev. 164, 1–24.

Liu, L.Y., Lin, C.S., Jiang, L., Chen, Z.Y., 2000. Characteristics of Tertiary inversion structures and their influence on oil-gas accumulation in Xihu Trough, East China Sea. Acta Geosci. Sin. 21 (4; ISSU 60), 350–355 (in Chinese with English Abstract).

Liu, Y., Hu, Z., Gao, S., Günther, D., Xu, J., Gao, C., et al., 2008. In situ, analysis of major and trace elements of anhydrous minerals by la-icp-ms without applying an internal standard. Chem. Geol. 257 (1), 34–43.

Lopez-Sanchez, M.A., Aleinikoff, J.N., Marcos, A., Martínez, F.J., Llana-Fúnez, S., 2016. An example of low-Th/U zircon overgrowths of magmatic origin in a late orogenic Variscan intrusion: the San Ciprián massif (NW Spain). J. Geol. Soc. 173 (2), 282–291.

McLennan, S.M., Hemming, S., McDaniel, D.K., Hanson, G.N., 1993. Geochemical Approaches to Sedimentation, Provenance, and Tectonics. Special Papers-Geological Society of America, pp. 21.

Morley, C.K., Nelson, R.A., Patton, T.L., Munn, S.G., 1990. Transfer zones in the East African rift system and their relevance to hydrocarbon exploration in rifts (1). AAPG (Am. Assoc. Pet. Geol.) Bull. 74 (8), 1234–1253.

Morton, A.C., Hallsworth, C., 1994. Identifying provenance-specific features of detrital heavy mineral assemblages in sandstones. Sediment. Geol. 90, 241–256.

Morton, A.C., Hallsworth, C.R., 1999. Processes controlling the composition of heavy mineral assemblages in sandstones. Sediment. Geol. 124 (1–4), 3–29.

Morton, A.C., Hallsworth, C.R., Chalton, B., 2004. Garnet compositions in Scottish and Norwegian basement terrains: a framework for interpretation of North Sea sandstone provenance. Mar. Petrol. Geol. 21, 393–410.

Morton, A.C., Whitham, A.G., Fanning, C.M., 2005. Provenance of Late Cretaceous–Paleocene submarine fan sandstones in the Norwegian Sea: integration of heavy mineral, mineral chemical and zircon age data. Sediment. Geol. 182, 3–28.

Nelson, R.A., Patton, T.L., Morley, C.K., 1992. Rift-segment interaction and its relation to hydrocarbon exploration in continental rift systems (1). AAPG Bull. 76 (8), 1153–1169.

Northrup, C.J., Royden, L.H., Bucrhfiel, B.C., 1995. Motion of the Pacific Plate relation to Eurasia and its potential relation to Cenozoic extension along the eastern margin of Eurasia. Geology 23, 719–722.
Pan, B., Pang, H., Gao, H., Garzanti, E., Zou, Y., Liu, X., et al., 2016. Heavy-mineral analysis and provenance of yellow river sediments around the China loess plateau. J. Asian Earth Sci. 127, 1–11.
Paull, C., Greene, H., Ussler, W., Mitts, P., 2002. Pesticides as tracers of sediment transport through Monterey Canyon. Geo Mar. Lett. 22 (3), 121–126.
Qin, L.Z., Liu, J.S., Li, S., Z, H., Chang, Y.S., 2017. Characteristics of zircon in the Huagang Formation of the ccentral inversion zone of Xihu Sag and its provenance indication. Pet. Geol. Exp. 4, 010 (in Chinese with English abstract).
Sun, W.D., Ding, X., Hu, Y.H., Li, X.H., 2007. The golden transformation of the Cretaceous plate subduction in the west Pacific. Earth Planet Sci. Lett. 262 (3–4), 533–542.
Tao, R.M., 1994. Discussion on basin formation mechanism and basin types in east China sea continental Shelf Basin on west Pacific plate tectonics. China Offshore Oil Gas (1), 14–20 (in Chinese with English Abstract).
Tang, Y., Zhang, Y., Tong, L., 2017. Provenance of middle to late triassic sedimentary rocks in the zoige depression in the NE part of the Songpan–Ganzi flysch basin: petrography, heavy minerals, and zircon U–Pb geochronology. Geol. J. 52 (S1), 449–462.
Wang, C., Liang, X., Foster, D.A., Xie, Y., Tong, C., Pei, J., et al., 2016. Zircon U-Pb geochronology and heavy mineral composition constraints on the provenance of the middle Miocene deep-water reservoir sedimentary rocks in the Yinggehai-Song Hong Basin, South China Sea. Mar. Petrol. Geol. 77, 819–834.
Wang, G.C., 2003. A discussion on some focal problems of petroleum exploration in East China Sea basin. China Offshore Oil Gas 17 (1), 29–32 (in Chinese with English Abstract).
Wang, P., Zhao, Z.G., Zhang, G.C., Zhang, J.W., 2011. Analysis on structural evolution in Diaoyu Islands folded-uplift belt, East China Sea basin and its impact on the hydrocarbon exploration in Xihu Sag. Geol. Sci. Technol. Inf. 30 (4), 65–72.
Wang, W.J., Zhang, Y.G., Zhang, J.P., 2014. Seismic facies features and sedimentary facies distribution of oligocene Huagang Formation in xihu sag, east China sea basin. Mar. Orig. Petrol. Geol. 19 (1), 60–68 (in Chinese with English abstract).
Wiedenbeck, M., Allé, P., Corfu, F., Griffin, W.L., Meier, M., Oberli, F., et al., 1995. Three natural zircon standards for u-th-pb, lu-hf, trace element and ree analyses. Geostand. Newsl. 19 (1), 1–23.
Wu, F.D., Lu, Y.C., Chen, P., Zhou, P., 1997. The discovery and significance of glauconites in the huagang formation of the oligocene, xihu depression, east China sea. Acta Sedimentol. Sin. 15 (3), 158–161 (in Chinese with English Abstract).
Wu, L., Mei, L., Liu, Y., Luo, J., Min, C., Lu, S., et al., 2017. Multiple provenance of rift sediments in the composite basin-mountain system: constraints from detrital zircon U-Pb geochronology and heavy minerals of the early Eocene Jianghan Basin, central China. Sediment. Geol. 349, 46–61.
Xu, F., 2012. Characteristics of Caenozoic structure and tectonic migration of the east China Sea Shelf basin. J. Oil Gas Technol. 34 (6), 1–7 (in Chinese with English Abstract).
Xu, Y.X., Hu, M.Y., Liang, J.S., KE, L., Jiang, H.U., 2010. Sedimentary provenance analysis of oligocene Huagang Formation in xihu sag of east China sea basin. J. Oil Gas Technol. 5, 042 (in Chinese with English abstract).
Yang, F.L., Xu, X., Zhao, W.F., Sun, Z., 2011. Petroleum accumulations and inversion structures in the xihu depression, east China sea basin. J. Petrol. Geol. 34 (4), 429–440.
Yang, Q.L., 1992. Geotectonic framework of the east China sea. In: In: Watkins, J.S., Zhiqiang, F.K., McMillen, J. (Eds.), Geology and Geophysics of Continental Margins, vol 53. Am Assoc Pet Geol Mem, pp. 17–25.
Yang, S., Hu, S., Cai, D., Feng, X., Chen, L., Gao, L., 2004. Present-day heatflow, thermal history and tectonic subsidence of the East China Sea Basin. Mar. Petrol. Geol. 21, 1095–1105.
Yang, W., Cui, Z., Zhang, Y., 2010. Geology & Minerals of East China Sea. China Ocean Press, Beijing (in Chinese).
Yang, X.H., Li, A.C., Qin, Y.S., Wu, S.G., Wu, Z.X., Zhang, J.P., 2006. U-Pb dating of zircons from cenozoic sandstone: Constrain on the Geodynamic setting of east China Sea Shelf basin. Mar. Geol. Quat. Geol. 26 (3), 75–86 (in Chinese with English abstract).
Ye, J., Qing, H., Bend, S.L., Gu, H., 2007. Petroleum systems in the offshore xihu basin on the continenal shelf of the east China sea. AAPG Bull. 91 (8), 1167–1188.
Zhang, J., Xu, F., Zhong, T., Zhang, T., Yu, Y., 2012. Sequence stratigraphic models and sedimentary evolution of pinghu and huagang formations in xihu trough. Mar. Geol. Quat. Geol. 32 (1), 35–42 (in Chinese with English Abstract).
Zhao, H.M., Lv, B.Q., Sun, H.B., Wang, H.G., Xu, G.Q., 2002. Formation and evolution of marginal basins in the western pacific. Mar. Geol. Quat. Geol. 22 (1), 57–62 (in Chinese with English Abstract).
Zheng, Q.G., Zhou, Z.Y., Cai, L.G., Lu, Y.D., Cao, Q.G., 2005. Meso-cenozoic tectonic setting and evolution of east China sea shelf basin. Oil Gas Geol. 26 (2), 197–201 (in Chinese with English Abstract).
Zhou, Z., Zhao, J., Yin, P., 1989. Characteristics and tectonic evolution of the east China sea. In: Zhu, X. (Ed.), Chinese Sedimentary Basins: Sedimentary Basins of the World 1. Elsevier, Amsterdam, pp. 165–179.
Zhu, W., 2010. Altas of Oil and Gas Basins, China Sea. Petroleum Industry Press, Beijing, pp. 73–75 (in Chinese).
Zhu, W., Wu, C., Wang, J., Zhou, T., Li, J., Zhang, C., Li, L., 2017. Heavy mineral compositions and zircon U-Pb ages of Cenozoic sandstones in the SW Qaidam basin, northern Tibetan Plateau: implications for provenance and tectonic setting. J. Asian Earth Sci. 146, 233–250.